*Pre-Print*
**of the original manuscript:**

Oliveira, J.P.; Cavaleiro, A.J.; Schell, N.; Stark, A.; Miranda, R.M.; Ocana, J.L.; Braz Fernandes, F.M.:

**Effects of laser processing on the transformation characteristics of NiTi: A contribute to additive manufacturing**

In: Scripta Materialia 152 (2018) 122 - 126
First published online by Elsevier: April 27, 2018

DOI: 10.1016/j.scriptamat.2018.04.024
https://dx.doi.org/10.1016/j.scriptamat.2018.04.024

# Effects of laser processing on the transformation characteristics of NiTi: a contribute to additive manufacturing

J. P. Oliveira [1, 2, 3 *], A. J. Cavaleiro [4, 5], N. Schell [6], Andreas Stark [6], R. M. Miranda [3], J. L. Ocana [7], F. M. Braz Fernandes [1]

[1] – CENIMAT/i3N, Faculdade de Ciências e Tecnologia, Universidade Nova de Lisboa, Portugal

[2] – Department of Materials Science and Engineering, The Ohio State University, 1248 Arthur E. Adams Drive, Columbus, OH 43221, USA

[3] – UNIDEMI, Departamento de Engenharia Mecânica e Industrial, Faculdade de Ciências e Tecnologia, Universidade Nova de Lisboa, Caparica, Portugal

[4] – CEMMPRE Centre for Mechanical Engineering, Materials and Processes, Group of Nanomaterials and Micromanufacturing, Department of Mechanical Engineering, University of Coimbra, 3030-201, Coimbra, Portugal

[5] – INEGI Instituto de Ciência e Inovação em Engenharia Mecânica e Engenharia Industrial − INEGI, Porto, Portugal

[6] – Institute of Materials Research, Helmholtz-Zentrum Geesthacht, Max-Planck-Str. 1, D-21502 Geesthacht, Germany

[7] – Centro Láser UPM, Universidad Politécnica de Madrid, Edificio "La Arboleda", Ctra. Valencia, km 7,300, Campus Sur UPM, 28031 Madrid, Spain

* – corresponding author: jp.oliveira@campus.fct.unl.pt

## Abstract

Laser additive manufacturing of NiTi generates complex microstructural features not fully understood yet. Thermal similarities between laser microjoining and laser additive manufacturing, enables correlating the effect of the laser on the material in both processes. To clarify them, a simplified yet accurate approach was employed: in-situ X-ray diffraction was used to determine the local transformation temperatures along the thermally affected regions in a laser processed NiTi thin sheet. The observed gradient of transformation temperatures is related to local chemical compositional changes through Ni depletion, and residual stresses explaining the peculiar microstructural and mechanical features observed in additive manufacturing of NiTi.

**Keywords**: Laser welding; Synchrotron radiation; Shape memory alloys (SMA); Phase transformation; Additive manufacturing.

Laser additive manufacturing (AM) of NiTi shape memory alloys (SMAs) is currently a topic which attracts significant attention from both academia and industry [1].

Laser AM of NiTi has been studied by several authors focusing on the understanding of effect of process parameters, mechanical performance and potential applications [2–9]. However, despite the significant interest in laser AM for NiTi there are some microstructural features occurring due to the laser/material interaction effects that are not fully understood yet. One example is that in differential scanning calorimetry (DSC) analysis of AM NiTi parts the transformation peaks tend to be broad, meaning that the transformation temperatures spread over a relatively large range of temperatures [3,5,9]. On the other hand, when a conventional and homogenous sample is analyzed, the transformation peaks are usually sharper and well-defined [10,11].

Another typical characteristic in laser AM of NiTi is the usual requirement for solution annealing heat treatments [3,4,12]. Although the reason for such need is not discussed in detail, it can be assumed that this is related to the presence of nanometric precipitates which are formed during the AM process due to the thermal history of the material [5,6,8]. Since these precipitates are not expected to be evenly distributed along the material, solution annealing would allow dissolving them into the matrix, thus homogenizing the microstructure of the parts. This justifies the improved mechanical and functional properties of AM parts after solution annealing [4,12]. After homogenization of the microstructure in as-solubilized parts, conventional heat treatments (such as ageing) can be performed, and the mechanical behavior is reported to be more stable and homogenous [13]. This can be attributed to the uniform distribution of precipitates that can occur in the material: after solution annealing, precipitates formed during the AM process will be dissolved into the matrix, thus allowing that any subsequent heat treatment induces a homogenous precipitation along the fabricated part.

Alongside with DSC analysis [14–16], X-ray diffraction (XRD) with temperature variation [17–20] is also widely used to determine the transformation characteristics of NiTi. However, in laser AM each deposited layer is very small (in the order of dozens of micrometers), which results in a significant difficulty to analyze only one deposited layer. Since NiTi is extremely sensitive to high temperatures, two consecutive deposited layers may not have the same microstructural characteristics, since their thermal history will differ. This feature, combined with the difficulty to isolate a single deposited layer for determination of the transformation characteristics of the material, make it prone for the superimposition of microstructural information coming from multiple deposited layers, which may mask the actual transformation characteristics of a specific region of the material.

Based on these limitations, it is clear the need for a simplified approach to fully understand the effects on the microstructure, namely the transformation temperatures, of AM NiTi parts. One way to for such simplified approach is trough establishing a parallel analysis with laser welding/processing of thin plates. In both laser (micro)welding and laser-based AM where fusion occurs, a small heat source rapidly scans the material. During welding, the heat source promotes localized melting to join parts. In AM the laser scans the substrate to create the desired structure [21–23]. The main difference between laser welding and laser AM is that in the former, the laser only scans the material once, while in the latter the laser scanning remelts the material several times creating numerous heat affected zones (HAZ) that will be superimposed as the number of deposited layers increases. Since AM can be considered as a superimposition of several HAZ and FZ (as more and more layers are deposited) it is possible to gain knowledge on the process effects by performing conventional laser material processing, as in laser welding. In fact, the HAZ and FZ of a laser weld can be compared to two successive deposited layers in AM: the last layer has a structure similar to the FZ, inducing in the precedent a thermally affected zone that can be viewed as a HAZ. Therefore, with such approach, one is simplifying the effect of multiple repasses, as it occurs in laser AM, still generating an important understanding of the microstructural induced effects of the process on the transformation temperatures along the different regions of the material.

Laser welding of NiTi is widely reported in the literature, with different studies addressing the effects of this joining technique on the microstructure and functional properties [24–39].

So far, the transformation characteristics in AM NiTi parts have been studied only with DSC which presents some problems as detailed previously. In-situ scanning and transmission electron microscopy (SEM/TEM), with the former supported by electron backscattered diffraction (EBSD) can also be used to analyze the transformation characteristics of NiTi [40–43]. Each technique has its own advantages/disadvantages and length scale of application. Since the thermally affected regions in laser processed NiTi may span several hundred microns, TEM analysis would not be ideal due to the need to prepare several foils, which would only provide a very localized information of the phase transformation characteristics experienced by the material instead of a more global view. EBSD does not have the length restriction to fully analyze the HAZ and FZ, but requires extensive sample preparation and only provides surface information, although the resolution can reach the nanometer range. A potential solution to understand the thermal history induced by the laser processing on the transformation characteristics of laser processed NiTi is using synchrotron X-ray diffraction (SXRD). The spatial resolution can be on the micrometer range, since the extremely large photon flux allows to decrease the radiation spot while maintaining fast acquisition rates. This ability to tune the spatial resolution enables a more comprehensive analysis of the transformation behavior along laser processed parts. Additionally, SXRD working in transmission provides bulk information rather than only surface information.

To bring some light into the effects of laser AM on the transformation characteristics of NiTi SMAs, a simplified approach was used: a laser beam scanned a NiTi thin sheet to create a HAZ and FZ; then, the transformation temperatures along the different regions of the material were determined by in-situ SXRD, in transmission mode, with a small spot size. The results put in evidence the effect of the thermal history on the material and justify some of the singularities reported in the microstructure and mechanical behavior of AM NiTi parts.

50.8Ni-Ti (at. %) plates, 0.5 mm thick, austenitic at RT and supplied in the flat annealed condition, were laser scanned using a continuous wave Nd:YAG laser. The laser parameters were a power of 726 W and a travel speed of 30 mm/s. The laser beam diameter was of 0.45 mm with Argon used as shielding gas.

SXRD was used to probe the laser processed sample after cutting and polish a strip of material with 5 mm in length and 2.5 mm wide. Measurements were performed at P07 beamline at DESY synchrotron. A beam spot of 100 x 100 µm, with a 100 µm step increase, probed the welded material starting in the base material (BM) up to the weld centerline, taking advantage of the symmetry along this centerline. 11

consecutives scans were necessary to probe all these regions consecutively. The weld cross-section was positioned perpendicular to the X-ray beam, allowing to analyze regions of the material that are homogenous along the X-ray beam path. A schematic representation of the measurements is depicted in Figure 1 a. A beam energy of 99 keV (0.12525 Å) and an exposure time of 0.5 seconds for each analyzed spot allows to integrate the material relatively fast and with an excellent peak/background ratio. SXRD measurements were performed while heating the sample from RT (23 $^{o}$C) and up to 150 $^{o}$C using an induction heating furnace. A slow heating rate of 2 K/min was used so that each sequence of 11 consecutive scans could be performed at the same temperature ensuring a precision of ± 1 K. A 2D detector 1430 mm away from the sample was used to collect the Debbye-Scherrer rings. This geometry allows to integrate a small volume along the weld direction, revealing the true phase distribution along the HAZ and FZ with the resolution that is the most adequate for a clear identification of the structural gradient. Raw data images were treated using Fit2d [44,45].

The superimposition of the SXRD patterns (Figure 1 b) from the BM to the weld centerline taken at RT clearly reveal the effect of laser processing on the microstructure: while the BM is fully austenitic, in the HAZ and FZ a mixture of martensite and austenite is observed.

To clearly determine at which temperature the martensite to austenite transformation occurs, it was selected to analyze the (010) martensite peak, located at $2\theta = 1.57^{o}$, since there are no other peaks in its neighborhood that may result in misinterpretation of results. To simplify these observations, only characteristic scans of distinct regions of the processed NiTi were analyzed, as detailed in Table 1.

**Table 1 – Regions of interest analyzed during the in-situ measurements of laser processed NiTi.**

| Scan ID | Analyzed Region |
|---|---|
| **A** | Base material – **BM** |
| **B** | Heat affected zone near base material – **HAZ/BM** |
| **C** | Middle of the heat affected zone – **HAZ** |
| **D** | Fusion zone near the heat affected zone – **FZ/HAZ** |
| **E** | Weld centerline – **FZ** |

Figure 2 depicts the evolution of the (010) martensite peak during heating to 150 $^{o}$C. Except for 23 and 40 $^{o}$C (Figures 2 a and b, respectively), all temperatures shown correspond to those where the (010) martensite peak disappeared in any of the regions detailed in Table 1, thus indicating that the martensite to austenite transformation occurred.

At RT, all regions but the non-affected BM have martensite (Figure 2 a). The intensity of the martensite peak for each position is related to the martensite content, thus confirming the presence of a phase gradient throughout the processed material.

The $A_f$ temperature of the BM was 10 $^{o}$C. However, at 40 $^{o}$C martensite was still present in all regions of the HAZ and FZ (Figure 2 b). Only at 57 $^{o}$C the first martensite to austenite transformation takes place and this occurred in the HAZ near the BM (Figure 2 c).

The next thermal induced transformation is observed in the middle of the HAZ at 73 $^oC$ (Figure 2 d). The distance between the HAZ near the BM and the middle of the HAZ was nearly 200 µm. Within this region the thermal cycle experienced by both regions during laser processing was sufficient for a difference in the transformation temperature of 16 K.

The complete transformation from martensite to austenite at the HAZ/FZ interface only occurred at 107 $^oC$ (Figure 2 e), meaning that the thermal cycle experienced in this region had a more pronounced microstructural influence in the transformation temperatures. Finally, the weld centerline, which experiences the highest temperature during welding, fully transforms to austenite at 141 $^oC$ (Figure 2 f).

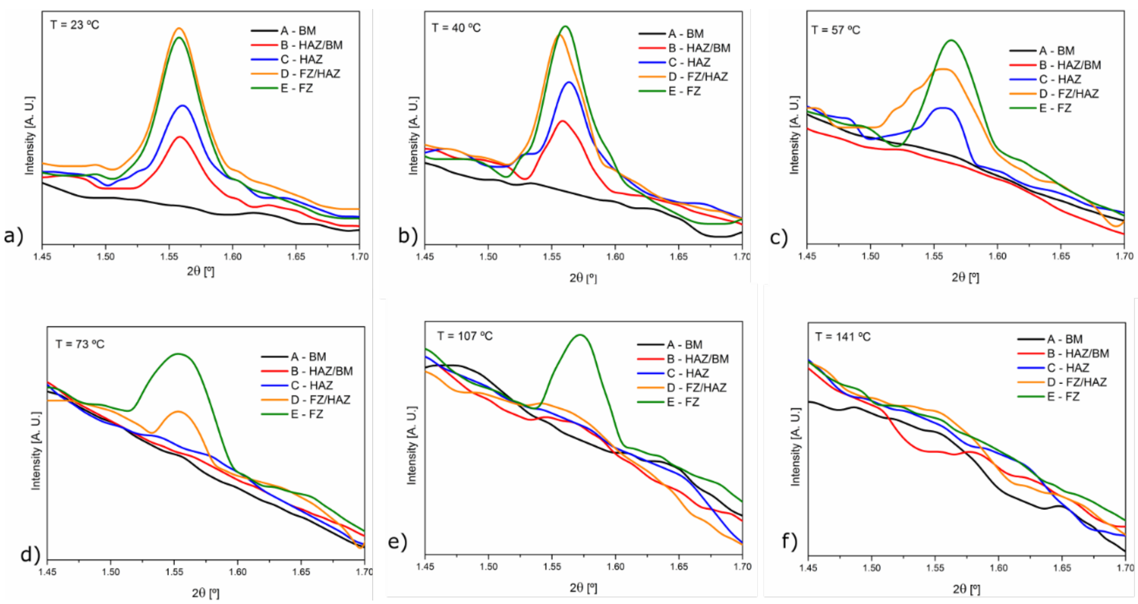


**Figure 1 – Diffractograms of the (010) martensite peak at different temperatures: a) at 23 $^oC$; b) at 40 $^oC$; c) 57 $^oC$; d) at 73 $^oC$; e) at 107 $^oC$; f) at 141 $^oC$. Each color of the plots corresponds to one of the locations detailed in Table 1.**

The reason for each region of the processed material to exhibit different transformation temperatures is mainly related to the phase content within the weld. The phase content variation is directly linked to changes of the Ni/Ti ratio on the metal matrix in both the HAZ and FZ. Transformation temperatures of Ni-rich NiTi alloys are extremely dependent on the chemical composition of the material [46]. In fact, an increase of 0.1 at % in Ni-rich NiTi is enough to decrease the transformation temperatures by 20 K [47]. Hence, any minor Ni depletion phenomena induced by laser processing can dramatically modify the transformation temperatures along the processed regions.

In a precedent paper it was shown that $Ni_4Ti_3$ precipitation occurs in the HAZ of NiTi laser welds [28]. To confirm if $Ni_4Ti_3$ the material was heated to 150 $^oC$, so that all martensite transforms to austenite. Thus, any remaining peaks will correspond to either austenite or precipitates, as at RT the broad peaks typical of martensite hinder the $Ni_4Ti_3$. Using 39-1113 JCPDF card it was possible to index $Ni_4Ti_3$ peaks, confirming its presence in the HAZ (Figure 1 c).

In Ni-rich NiTi, the precipitation of $Ni_4Ti_3$ can occur after just a few seconds at critical temperatures [48]. Even with the fast cooling rates typical of laser welding, the permanence time between 350 and 500 $^{o}C$ where $Ni_4Ti_3$ may precipitate, are still in the order of a couple of seconds [38], hence justifying its presence in the HAZ. On the FZ, no precipitation occurs since the permanence time at the critical temperatures for solid-state transformation is extremely short [38]. However, the extremely high temperatures reached during laser processing promote preferential Ni evaporation, owing to its higher vapor pressure, resulting in Ni depletion.

In a fundamental paper [49], it was shown that significant Ni depletion in Ni-rich NiTi can raise the transformation temperatures up to around 95 $^{o}C$. This means that, aside from Ni depletion, another factor is also contributing to an increase in the transformation temperatures along the HAZ and FZ of the laser processed material. For NiTi, it is known that residual stresses can increase the transformation temperatures [55,56]. For that reason, von Mises residual stresses were determined along the welded joint, at RT, similarly to [45,50], and are depicted in the insert of Figure 3. The residual stresses can reach up to a maximum 378 MPa in the FZ. The Clausius-Clapeyron relation for NiTi can be of 8 MPa/$^{o}C$ [51]. This translates into an increase of transformation temperatures by 46.6 $^{o}C$ at the centre of the FZ. Thus, the more significant change can be attributed to chemical composition changes.

A representation of the evolution of the transformation temperatures as a function of distance within the HAZ and FZ of the laser processed NiTi is depicted in Figure 3. The driving mechanisms that promote Ni depletion in laser processed NiTi have distinct effects in terms of the magnitude of the chemical change along the material, and therefore on the relative change of the transformation temperatures. In fact, the preferential evaporation effect in the FZ is much more efficient in promoting a Ni depletion, than the precipitation of $Ni_4Ti_3$ in the HAZ. For this reason, the transformation temperatures increase from the BM towards the weld centerline, in a similar trend as the Ni depletion increases.

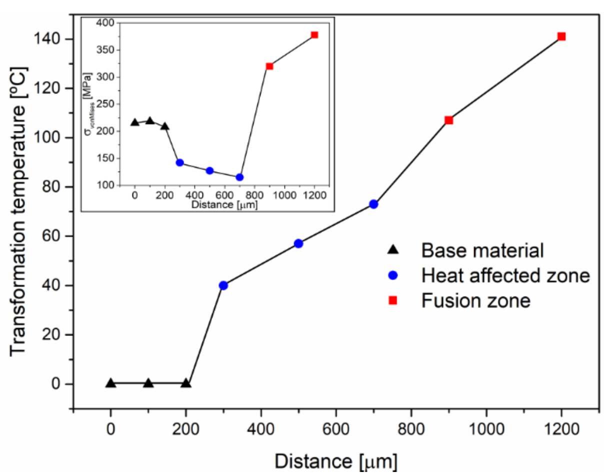


**Figure 2 – Evolution of the transformation temperatures in the BM, HAZ and FZ obtained from in-situ SXRD.**

To the best of the authors knowledge, no other research experiments were performed on laser processed NiTi, making use of such spatial resolution for the determination of the transformation temperatures along the processed regions. These results bring some light into the previously described microstructural and mechanical features that occur in AM of NiTi. In particular, the presence of precipitates unevenly distributed along AM NiTi parts [5,6,8] can justify both the widening of the DSC peaks in as-build parts and the need for solution annealing heat treatments. In the first case, the widening of the peaks can be justified by the fact that the analyzed material exhibits a gradient of transformation temperatures, as it was evidenced in this work. In the second case, solution annealing allows dissolving any precipitates formed during the process and that can drastically change the transformation characteristics of the material.

For this class of alloys, solution annealing of AM parts is even more important since two competing mechanisms will influence the mechanical behavior of the part: inhomogeneous precipitation and residual stress build up. Assuming that the process can promote random precipitation of phases during the process, as described in the literature [5,6], a local change of the transformation characteristics and therefore in the mechanical behavior is expected. During AM, the multiple laser scans promote heat accumulation effects, exposing the part to critical temperatures and during permanence times where such solid-state phenomena can occur. However, the scan strategy itself will imply that different regions within the same deposited layer will have different thermal cycles, which contributes for a non-homogenous precipitate distribution along the part.

The presence of precipitates that are reported to occur in AM NiTi parts, alongside with preferential evaporation occurring in the melt pool during the process, may cause compositional gradients that will result in a gradient of transformation temperatures. These microstructural changes, even when occurring at a small scale, as in both laser processing and laser AM, may significantly impact the transformation behavior of different regions, as evidenced by the in-situ measurements presented in this work, and therefore the functional properties of the material.

According to the results presented here, it is also possible to understand the importance of solution annealing heat treatments typically performed in AM NiTi parts. The dissolution of precipitates that are heterogeneously distributed throughout the built part, followed by conventional heat treatments (such as ageing) used for NiTi SMAs, will induce homogeneous precipitation along the part [13]. This is evidenced by sharper transformation peaks during DSC [4] and improvements in the mechanical behavior. Furthermore, these heat treatments typically promote stress relief in the material, which is also advantageous to decrease the transformation temperature of the parts.

In this work, a 100 $\mu$m resolution in-situ SXRD was performed to analyze the transformation temperatures along laser processed NiTi. The objective was to clarify some of the microstructural features observed by other authors in laser AM of NiTi [2,4,6] and its influence on the transformation characteristics along the material.

The transformation temperatures along the laser processed region are highly influenced by the process and thermal cycle: while the BM is fully austenitic at RT, the middle of the HAZ and the weld centerline only transformed to austenite at 73 and 141 $^{o}$C, respectively. Ni depletion through Ni-rich precipitation in the HAZ and preferential Ni evaporation in the FZ are the main factors accounting for these changes. Residual stress development in the laser welded joint also justifies part of the increase in the transformation temperatures of the joint.

These results were used to gain more knowledge on the effects of laser AM to produce NiTi SMAs, owing to the intrinsic similarities between laser processing, as it was performed in this work, and laser AM. A comparison of key literature in AM of NiTi with these new results was presented to provide a more fundamental understanding of the microstructural singularities observed in AM parts and its relation to the phase transformation characteristics.

JPO and FMBF acknowledge funding by National Funds through the Portuguese Foundation for Science and Technology (FCT-MCTES), Reference UID/CTM/50025/2013 and FEDER funds through the COMPETE 2020 Programme under the project number POCI-01-0145-FEDER-007688. AJC acknowledges funding by FCT under the projects PEst-C/EME/UI0285/2013 (CEMUC) and FEDER funds through the program COMPETE Programa Operacional Factores de Competitividade under project CENTRO-07-0224-FEDER-002001 “MT4MOBI − Materials and Technologies for Greener Manufacturing & Products Applied to Mobility” and SciTech Science and Technology for Competitive and Sustainable Industries, R&D project co-financed by Programa Operacional Regional do Norte (“NORTE2020”). RMM acknowledges FCT-MCTES for its financial support via the project PEst-OE/EME/UI0667/2014 (UNIDEMI). JPO acknowledges FCT-MCTES for funding PhD grant SFRH/BD/85047/2012. The authors acknowledge DESY for reimbursement of travel expenses and delivering beam under proposal I-20120563 EC. The authors acknowledge Dr. Petr Šittner from Academy of Sciences of the Czech Republic for the useful discussions.

[1] M. Elahinia, N. Shayesteh Moghaddam, M. Taheri Andani, A. Amerinatanzi, B.A. Bimber, R.F. Hamilton, Prog. Mater. Sci. 83 (2016) 630–663.

[2] R.F. Hamilton, B.A. Bimber, M. Taheri Andani, M. Elahinia, J. Mater. Process. Technol. 250 (2017) 55–64.

[3] C. Haberland, M. Elahinia, J.M. Walker, H. Meier, J. Frenzel, Smart Mater. Struct. 23 (2014) 104002.

[4] S. Saedi, A.S. Turabi, M.T. Andani, C. Haberland, H. Karaca, M. Elahinia, J. Alloys Compd. 677 (2016) 204–210.

[5] B.E. Franco, J. Ma, B. Loveall, G.A. Tapia, K. Karayagiz, J. Liu, A. Elwany, R. Arroyave, I. Karaman, Sci. Rep. 7 (2017) 3604.

[6] J. Ma, B. Franco, G. Tapia, K. Karayagiz, L. Johnson, J. Liu, R. Arroyave, I. Karaman, A. Elwany, Sci. Rep. 7 (2017) 46707.

[7] R.F. Hamilton, T.A. Palmer, B.A. Bimber, Scr. Mater. 101 (2015) 56–59.

[8] B.A. Bimber, R.F. Hamilton, J. Keist, T.A. Palmer, Mater. Sci. Eng. A 674 (2016) 125–134.

[9] S. Shiva, I.A. Palani, S.K. Mishra, C.P. Paul, L.M. Kukreja, Opt. Laser Technol. 69 (2015) 44–51.

[10] C. Tang, W.M. Huang, C.C. Wang, H. Purnawali, Smart Mater. Struct. 21 (2012) 85022.

[11] Y. Xiao, P. Zeng, L. Lei, Mater. Res. Express 3 (2016) 105701.

[12] S. Saedi, A.S. Turabi, M.T. Andani, N.S. Moghaddam, M. Elahinia, H.E. Karaca, Mater. Sci. Eng. A 686 (2017) 1–10.

[13] S. Saedi, A.S. Turabi, M.T. Andani, C. Haberland, M. Elahinia, H. Karaca, Smart Mater. Struct. 25 (2016) 35005.

[14] T.G. Bradley, W. a Brantley, B.M. Culbertson, Am. J. Orthod. Dentofacial Orthop. 109 (1996) 589–597.

[15] M.F.X. Wagner, S.R. Dey, H. Gugel, J. Frenzel, C. Somsen, G. Eggeler, Intermetallics 18 (2010) 1172–1179.

[16] Y.Y. Liu, Y.Y. Liu, J. Van Humbeeck, J.V.A.N. Humbeeck, Acta Mater. 47 (1998) 199–209.

[17] Z. Bojarski, H. Morawiec, in:, X-Ray Neutron Struct. Anal. Mater. Sci., Springer US, Boston, MA, 1989, pp. 43–48.

[18] M. Pattabi, K. Ramakrishna, K.K. Mahesh, Mater. Sci. Eng. A 448 (2007) 33–38.

[19] M. Honarvar, B. Konh, T.K. Podder, A.P. Dicker, Y. Yu, P. Hutapea, J. Mater. Eng. Perform. 24 (2015) 3038–3048.

[20] E. Polatidis, N. Zotov, E.J. Mittemeijer, Powder Diffr. 30 (2015) S76–S82.

[21] T. DebRoy, H.L.L. Wei, J.S.S. Zuback, T. Mukherjee, J.W.W. Elmer, J.O.O. Milewski, A.M.M. Beese, A. Wilson-Heid, A. De, W. Zhang, Prog. Mater. Sci. 92 (2018) 112–224.

[22] T.M. Mower, M.J. Long, Mater. Sci. Eng. A 651 (2016) 198–213.

[23] A. Zinoviev, O. Zinovieva, V. Ploshikhin, V. Romanova, R. Balokhonov, Mater. Des. 106 (2016) 321–329.

[24] J.P. Oliveira, R.M. Miranda, F.M. Braz Fernandes, Prog. Mater. Sci. 88 (2017) 412–466.

[25] A. Tuissi, S. Besseghini, T. Ranucci, F. Squatrito, M. Pozzi, Mater. Sci. Eng. A 273–275 (1999) 813–817.

[26] J.P. Oliveira, R.M. Miranda, N. Schell, F.M. Braz Fernandes, Int. J. Fatigue 83 (2016) 195–200.

[27] Y.G.G. Song, W.S.S. Li, L. Li, Y.F.F. Zheng, Mater. Lett. 62 (2008) 2325–2328.

[28] J.P. Oliveira, F.M. Braz Fernandes, R.M. Miranda, N. Schell, J.L. Ocaña, Mater. Charact. 119 (2016) 148–151.

[29] H. Gugel, A. Schuermann, W. Theisen, Mater. Sci. Eng. A 481–482 (2008) 668–671.

[30] J.P. Oliveira, B. Panton, Z. Zeng, T. Omori, Y. Zhou, R.M. Miranda, F.M. Braz Fernandes, Mater. Des.

90 (2016) 122–128.

[31] R. Hahnlen, G. Fox, M.J. Dapino, J. Intell. Mater. Syst. Struct. 24 (2012) 945–961.

[32] C.W. Chan, H.C. Man, F.T. Cheng, Mater. Sci. Eng. A 559 (2013) 407–415.

[33] A. Falvo, F.M.M. Furgiuele, C. Maletta, Mater. Sci. Eng. A 481–482 (2008) 647–650.

[34] C. Maletta, A. Falvo, F. Furgiuele, G. Barbieri, M. Brandizzi, J. Mater. Eng. Perform. 18 (2009) 569–574.

[35] C.W. Chan, H.C. Man, T.M. Yue, Metall. Mater. Trans. A Phys. Metall. Mater. Sci. 42 (2011) 2264–2270.

[36] C.W. Chan, H.C. Man, Opt. Lasers Eng. 49 (2011) 121–126.

[37] B. Tam, M.I. Khan, Y. Zhou, Metall. Mater. Trans. A 42 (2011) 2166–2175.

[38] J.P. Oliveira, F.M. Braz Fernandes, R.M. Miranda, N. Schell, Shape Mem. Superelasticity 2 (2016) 114–120.

[39] J.P. Oliveira, F.M.B. Fernandes, N. Schell, R.M. Miranda, Mater. Lett. 171 (2016) 273–276.

[40] L. Tan, W.C.C. Crone, Scr. Mater. 50 (2004) 819–823.

[41] P. Nie, O.A.A. Ojo, Z. Li, Acta Mater. 77 (2014) 85–95.

[42] J. Rak, T. Goryczka, P. Ochin, Acta Phys. Pol. A 130 (2016) 1075–1078.

[43] S.C. Mao, J.F. Luo, Z. Zhang, M.H. Wu, Y. Liu, X.D. Han, Acta Mater. 58 (2010) 3357–3366.

[44] A.P. Hammersley, S.O. Svensson, M. Hanfland, A.N. Fitch, D. Hausermann, High Press. Res. 14 (1996) 235–248.

[45] J.P. Oliveira, F.M.B. Fernandes, R.M. Miranda, N. Schell, J.L. Ocaña, Mater. Des. 100 (2016) 180–187.

[46] K. Otsuka, X. Ren, Prog. Mater. Sci. 50 (2005) 511–678.

[47] J. Khalil Allafi, X. Ren, G. Eggeler, J.K. Allafi, X. Ren, G. Eggeler, J. Khalil Allafi, X. Ren, G. Eggeler, Acta Mater. 50 (2002) 793–803.

[48] A.R. Pelton, J. Dicello, S. Miyazaki, Minim. Invasive Ther. Allied Technol. 9 (2000) 107–118.

[49] J. Frenzel, E.P. George, A. Dlouhy, C. Somsen, M.F.-X. Wagner, G. Eggeler, Acta Mater. 58 (2010) 3444–3458.

[50] H.-R. Wenk, L. Lutterotti, P. Kaercher, W. Kanitpanyacharoen, L. Miyagi, R. Vasin, Powder Diffr. 29 (2014) 1–13.

[51] Y. Liu, H. Yang, Smart Mater. Struct. 16 (2007) S22–S27.